Inorg. Chem. **2004**, *43*, 1421−1428

Platinum Ion Uptake by Dendrimers: An NMR and AFM Study

Perry J. Pellechia,*,† Jinxin Gao,† Yunlong Gu,‡ Harry J. Ploehn,‡ and Catherine J. Murphy*,†

Department of Chemistry and Biochemistry, 631 Sumter Street, University of South Carolina, Columbia, South Carolina 29208, and Department of Chemical Engineering, Swearingen Engineering Center, University of South Carolina, Columbia, South Carolina 29208

Received September 27, 2003

The reaction of generation 2 and generation 4 poly(amidoamine) (PAMAM) dendrimers with K_2PtCl_4 was studied by several NMR methods. The time dependency of the Pt(II) complexation was followed with ^{195}Pt NMR for both dendrimers and the equilibrium product was further characterized with ^{1}H NMR, and indirectly detected ^{13}C NMR, in the case of the generation 2 dendrimer. After 2 days, a black precipitate of Pt(0) was observed, half the original ^{195}Pt signal was lost, and approximately 20% of the initial Pt(II) was coordinated to the tertiary and secondary nitrogens of the generation 2 dendrimer. The uptake of Pt(II) by the generation 4 dendrimer was much slower, consistent with the steric crowding of the surface groups on the generation 4 dendrimer compared to the more open generation 2. After 10 days, 80% of the Pt(II) was deep within the generation 4 dendrimer; the remaining 20% was unreacted or bound near the surface nitrogens of a single dendrimer. The location and time course of the platinum ion uptake by the dendrimers provides valuable insight into the formation of Pt^0 nanoparticles made in the presence of dendrimers as stabilizers, visualized by atomic force microscopy.

Introduction

Dendrimers are quasi-spherical, hyperbranched polymers with well-defined compositions and sizes.[1,2] Poly(amidoamine) (PAMAM) "Starburst" dendrimers are commercially available, and many workers have explored using these polymers as hosts to contain guests.[1,2] Particularly intriguing is the complexation of metal ions by PAMAM dendrimers to make metallic or semiconducting nanoparticles of controlled size and shape, either within dendrimers or between dendrimers.[1−15] Crooks has reported that metallic nanoparticles made within dendrimer matrixes are capable of doing selective catalysis based on the structure of the dendrimer host.[16]

Figure 1 shows the chemical structure of a generation 2 PAMAM dendrimer with terminal hydroxyl groups (G2-OH). We employ larger versions of these dendrimers (typically generation 4 and higher) to make Pt and other nanoparticles following published procedures.[1−15] To favor the uptake of Pt(II) precursor ions into the nitrogen-rich interior of PAMAM dendrimers, we chose the hydroxyl-terminated dendrimers instead of amine-terminated or carboxylic acid terminated dendrimers. The first step in the process is a slow ligand exchange reaction between the dendrimer and $[PtCl_4]^{2-}$ in aqueous solution, resulting in complexation of various Pt(II) species by the dendrimeric ligands.[1,6] (Presumably, of course, the nature of the Pt(II) precursor will affect the uptake, although we do not examine that here.) Treatment of the dendrimer−Pt(II) complex with $NaBH_4$ reduces the

* Authors to whom correspondence should be addressed. E-mail: pellechia@mail.chem.sc.edu (P.J.P.); murphy@mail.chem.sc.edu (C.J.M.).
† Department of Chemistry and Biochemistry.
‡ Department of Chemical Engineering.

(1) Crooks, R. M.; Zhao, M.; Sun, L.; Chechik, V.; Yeung, L. K. *Acc. Chem. Res*. **2001**, *34*, 181−190.
(2) Esumi, K. *Top. Curr. Chem*. **2003**, *227*, 31−52.
(3) Balogh, L.; Tomalia, D. A. *J. Am. Chem. Soc*. **1998**, *120*, 7355−7356.
(4) Zhao, M.; Sun, L.; Crooks, R. M. *J. Am. Chem. Soc*. **1998**, *120*, 4877−4878.
(5) Zhao, M.; Crooks, R. M. *Chem. Mater*. **1999**, *11*, 3379−3385.
(6) Zhao, M.; Crooks, R. M. *Adv. Mater*. **1999**, *11*, 217−220.
(7) Sooklal, K.; Hanus, L. H.; Ploehn, H. J.; Murphy, C. J. *Adv. Mater*. **1998**, *10*, 1083−1087.
(8) Huang, J.; Sooklal, K.; Murphy, C. J.; Ploehn, H. J. *Chem. Mater*. **1999**, *11*, 3595−3601.
(9) Sooklal, K.; Huang, J.; Murphy, C. J.; Hanus, L.; Ploehn, H. J. *Mater. Res. Soc. Symp. Proc*. **1999**, *576*, 439−444.
(10) Lakowicz, J. R.; Grycynski, I.; Grycynski, Z.; Murphy, C. J. *J. Phys. Chem. B* **1999**, *103*, 7613−7620.
(11) Hanus, L. H.; Sooklal, K.; Murphy, C. J.; Ploehn, H. J. *Langmuir* **2000**, *16*, 2621−2626.
(12) Lemon, B. I.; Crooks, R. M. *J. Am. Chem. Soc*. **2000**, *122*, 12886−12887.
(13) Esumi, K.; Suzuki, A.; Yamahira, A.; Torigoe, K. *Langmuir* **2000**, *16*, 2604−2608.
(14) Zhao, M.; Crooks, R. M. *Angew. Chem., Int. Ed*. **1999**, *38*, 364−366.
(15) Yeung, L. K.; Crooks, R. M. *Nano Lett*. **2001**, *1*, 14−17.
(16) Niu, Y.; Yeung, L. K.; Crooks, R. M. *J. Am. Chem. Soc*. **2001**, *123*, 6840−6846.

10.1021/ic035127e CCC: $27.50
Published on Web 01/28/2004

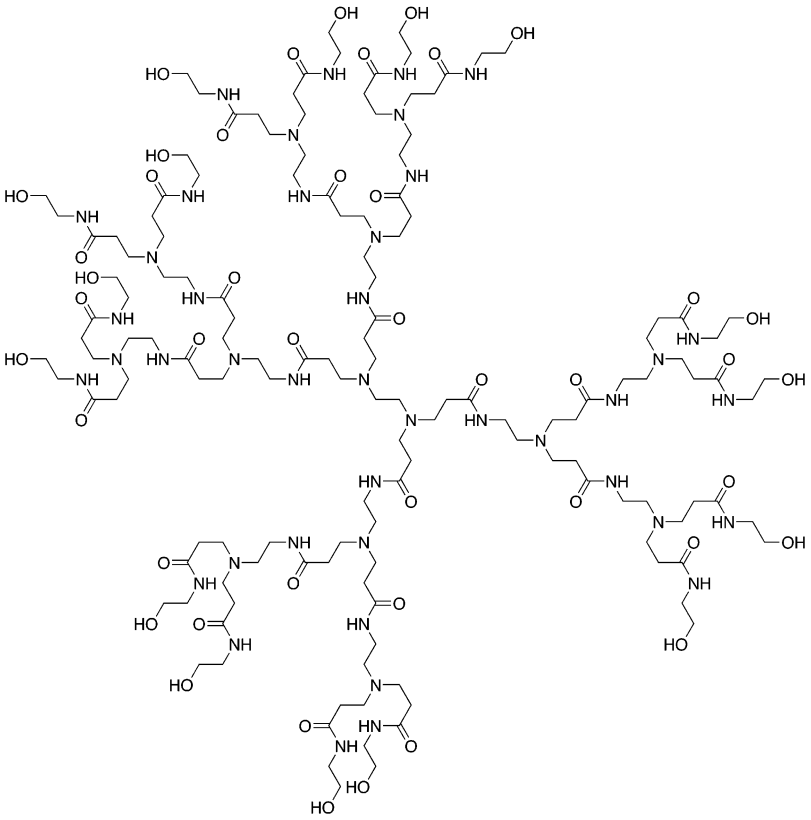

Figure 1. Chemical structure of a generation 2 PAMAM dendrimer bearing surface hydroxyl groups (G2-OH).

Pt to zero valence, ultimately resulting in Pt nanoparticles. The exact mechanism of nanoparticle formation is not definitively established. The prevailing view[1,6] is that the Pt nanoparticles are encapsulated by the dendrimer. Not only does the dendrimer stabilize the nascent particles against aggregation and bulk precipitation, but the dendrimer is also believed to serve as a template for nanoparticle formation: complexing a predetermined number of Pt(II) cations within the dendrimer leads to Pt nanoparticles containing that number of atoms.

We have been working to test this hypothesis. Clearly, the first critical step is the ligand exchange reaction between $[PtCl_4]^{2-}$ and PAMAM dendrimer. In this work, we describe the use of ^{195}Pt, ^{1}H, and ^{13}C NMR methods to elucidate the details of the ligand exchange reaction. Specifically, we use NMR to identify the speciation of the metal ions within the branches of the dendrimer, as well as track the progress of Pt uptake. This information will help us to interpret our observations of nanoparticle size distributions after reduction, leading to a better understanding of the nanoparticle formation mechanism.

Experimental Section

Materials and Synthesis. Potassium tetrachloroplatinate(II) (K_2PtCl_4, 99.9%), generation 2 PAMAM−OH dendrimer (G2-OH, 20 wt % solution in methyl alcohol), generation 4 PAMAM−OH dendrimer (G4-OH, 10 wt % solution in methyl alcohol), sodium borohydride ($NaBH_4$, 99%), and deuterium oxide (D_2O, 99.9 atom % D) were all purchased from Aldrich. Ultrapure deionized (DI) water was used for all sample preparations. All glassware was thoroughly cleaned with aqua regia and rinsed with DI water. To prepare a stock solution of PAMAM−OH, the required mass of dendrimer was obtained by weighing out as-purchased PAMAM methanol solution assuming 20 wt % G2-OH and 10 wt % G4-OH as specified by the manufacturer. Methanol was removed by stripping with flowing N_2 gas, followed by dissolution in DI water. Based on the intergration of ^{1}H NMR peaks, there was approximately one molecule of methanol per every dendrimer terminal group in solution in our experiments. These peaks were sharp in deuterated aqueous solution, consistent with the presence of "free" methanol, and not bound to the dendrimers. Dendrimer solutions were made up fresh for each synthesis. We observed no color changes or unusual peaks in the NMR experiments that would indicate actual chemical degradation of the dendrimers alone over the time course of our experiments.

The large hydrodynamic size of G4-OH leads to relatively slow rotational diffusion and unacceptable broadening of the NMR signal line widths. Thus the majority of the NMR experiments focused on Pt complexation with G2-OH. NMR samples were prepared by mixing 0.35 mL of 20 mM G2-OH, 0.35 mL of 200 mM K_2PtCl_4, and 0.07 mL of D_2O at room temperature in a 5 mm NMR tube. The resulting solutions were faint yellow (from the Pt(II) salt), with final concentrations of 0.09 M K_2PtCl_4, 0.009 M G2-OH, and 9.1% D_2O, and were used for NMR measurements immediately. These solutions have much higher concentrations of Pt than is typically used for Pt^0 nanoparticle synthesis. Over a period of 48 h, the solution turned dark brown, with some black precipitate presumed to be Pt^0. Overall, the ^{195}Pt signal was reduced by 50%. No further changes in color or NMR signal were observed after 48 h, indicating that equilibration was achieved. In the case of G4-OH experiments, the resulting solutions were also faint yellow, with final concentrations of 0.04 M K_2PtCl_4, 0.001 M G4-OH, and 9.1% D_2O; no precipitate was observed, but the overall ^{195}Pt signal was reduced by 80% after 10 days.

To make dendrimer−Pt^0 nanoparticles, low concentration solutions were prepared. To prepare G2-OH complexes with (nominally) 10 Pt(II) per dendrimer, equal volumes of 2 mM G2-OH and 20 mM K_2PtCl_4 stock solutions were mixed and stirred for 10 days. Over this period the solution color changed from light yellow to dark yellow. The final solution was 1 mM in G2-OH and 10 mM in Pt(II). The complexation of K_2PtCl_4 with G4-OH proceeded in a similar manner, except that the initial concentrations of the G4-OH and K_2PtCl_4 stock solutions were 0.2 and 8.0 mM, respectively, to attain a nominal ratio of 40 Pt(II) per G4-OH dendrimer. Equal volumes of the stock solutions were mixed and stirred for more than 10 days. Over this period the solution color changed from faint yellow to deep yellow. The final solution was 0.1 mM in G4-OH and 4.0 mM in Pt(II).

Atomic force microscopy (AFM) measurements focused on reduced G4-OH−Pt_{40} nanoparticles. To prepare reduced G4-OH−Pt_{40} (nominal), equal volumes of the G4-OH−Pt(II) complex solution and fresh 32 mM $NaBH_4$ stock solution were mixed and stirred for at least 1 h. A color change to dark yellow indicated the formation of Pt^0 nanoparticles. The final solution was 0.05 mM in G4-OH, 2.0 mM in Pt, and 16.0 mM in $NaBH_4$. The final solution was purified by dialysis for 3 days against pure DI water using cellulose dialysis tubing (Sigma, 1200 dalton cutoff) that had been soaked for 30 min in DI water prior to use. Reduction of similar dilute Pt complexes with G2-OH invariably led to an observable black precipitate. We prepared samples for AFM by diluting the purified nanoparticle solution with ultrapure water to achieve a G4-OH concentration of approximately 5×10^{-8} M. A drop of the diluted solution (2.5 μL) was deposited on the face of a freshly cleaved mica disk (grade V-4 muscovite, 9 mm diameter, SPM Inc.) and then air-dried in a covered dish at room temperature for at least 5 h.

NMR Methods. All NMR data were obtained at 25 °C using a Varian Inova 500 spectrometer operating at 500.215 MHz for proton. ^{195}Pt spectra were collected with a 5 mm broad-band probe tuned to 107.358 MHz. A 250 kHz spectral window was collected with 64 000 complex data points. Other parameters used include a relaxation delay of 10 ms, 45° pulse width (4.5 μs), and no proton decoupling. For the G2-OH complex study 96 000 transients were collected over 4 h for most acquisitions. The G4-OH reactions were carried out with a lower concentration of K_2PtCl_4 and required 24 h of data collection (576 000 transients). ^{195}Pt chemical shifts were externally referenced to K_2PtCl_6.

The very large spectral window used in the ^{195}Pt NMR experiments made it difficult to get even baselines and correct phase spectra with normal processing. This is caused by the fast digitization of the data and "dead time" between the rf pulse and receiver turnon.[18,19] To correct this problem, backfilling ("left shifts") of four points to the collected FIDs were performed using the linear prediction routine included in Varian's VNMR 6.1C software package. In fact, the first 20 points were calculated to correct nonideal receiver turnon. While this leads to flat baselines, it adds uncertainty to the peak intensities. Combined with the unlikely hood of uniform rf excitation across the large spectral window, the data were not treated quantitatively.

^{1}H and the indirectly detected ^{13}C data were collected with a 5 mm indirect detection probe that is equipped with a *z*-axis pulse field gradient coil. Presaturation of the dominant H_2O resonance was used for the single-dimension ^{1}H spectrum, but was not necessary for the gradient-enhanced two-dimensional experiments. The phase-sensitive gradient-enhanced double quantum filtered COSY (gDQCOSY) spectrum was obtained with a spectra width of 4 kHz, centered on the H_2O resonance that was assigned a value of 4.64 ppm. A single transient of 1000 complex data points was collected for each of 100 complex t_1 increments. The data were linear predicted with the Varian software up to 200 t_1 complex points, zero filled to 1000, and sine-bell weighted prior to Fourier transformation.

Both two-dimensional (2D) gradient-enhanced heteronuclear multiple-quantum correlation (gHMQC) spectra and 2D gradient-enhanced heteronuclear multiple-bond correlation (gHMBC) spectra were collected using a 4 kHz spectral window centered on the water resonance (4.64 ppm). Other common parameters include a 200 ppm t_1 (^{13}C) spectral width centered at 100 ppm that was collected with 256 magnitude value increments. GARP modulation was used for decoupling the ^{13}C doubles during acquisition of the gHMQC. The gHMQC required just two transients per increment, but more transients were needed for the gHMBC (12 for the dendrimer and 32 for Pt−dendrimer complex). Standard supplied pulse sequences were used in all cases.

AFM Methods. We used atomic force microscopy (AFM) to measure the vertical dimension of G4-OH−Pt_{40} nanoparticles deposited onto mica surfaces. All of the measurements employed a PicoSPM AFM system (Molecular Imaging, Inc.) operated in the tapping mode under ambient humidity and temperature conditions. We used standard silicon cantilevers (Ultrasharp NSC12/3, Mikromasch Inc.) having spring constants of 2.5−8.5 N/m and resonance frequencies between 120 and 190 kHz. According to the manufacturer, the probes have tip radii of about 10 nm. The vertical displacement of the piezo scan head was calibrated by the manufacturer to account for any nonlinearity. We performed additional calibrations with (nominal) 5 and 10 nm colloidal gold particles (Sigma).

Digital analysis of AFM images was performed using the SPIP software package (Image Metrology). This package performs appropriate background thresholding and automatic feature identification. For each distinct feature in the AFM image, the SPIP grain analysis module identifies the maximum *z*-value (height) associated with that feature. The height values obtained automatically via SPIP grain analysis agree well with the values for the same features measured manually using cross-section analysis provided by the PicoSPM operating software (PicoScan 5.2, Molecular Imaging). The maximal *z*-values for all features are compiled by SPIP and reported as a histogram. For each nanoparticle solution to be tested, we prepared at least three duplicate samples deposited on mica. Each mica surface was scanned over five distinct areas under the same operating conditions. In all cases, the resulting AFM images were found to be reproducible, as indicated quantitatively by comparing the maximal feature height histograms.

Results and Discussion

All of the NMR results reported here involve complexes of Pt(II) and its ligands with G2-OH and G4-OH dendrimers. We also present selected AFM results for reduced G4-OH−Pt_{40}.

^{195}Pt NMR Results for G2-OH. Within 12 h of the addition of K_2PtCl_4 to the aqueous G2-OH solution, several new peaks appear in the ^{195}Pt NMR spectrum. The $[PtCl_4]^{2-}$ resonance at −1617 ppm intensity drops, and peaks at −1878, −2133, and −2532 ppm grow in. Based on the

(17) Gu, Y.; Gao, J.; Xie, H.; Murphy, C. J.; Ploehn, H. J., manuscript in preparation.
(18) Pelczer, I.; Szalma, S. *Chem. Rev.* **1991**, *91*, 1507−1524.
(19) Hoult, D. I. *Prog. NMR Spectrosc.* **1978**, *12*, 41−77.

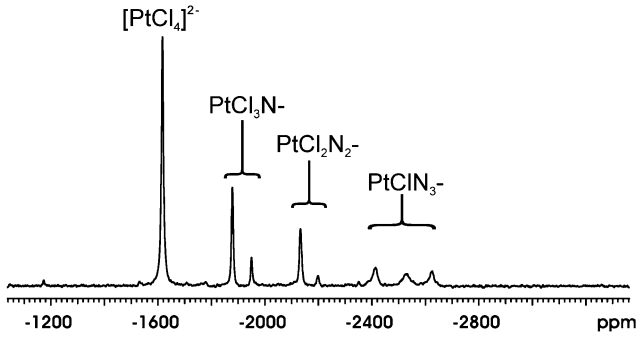

Figure 2. ^{195}Pt NMR spectrum of the complex formed between 0.09 M K_2PtCl_4 and 0.009 M G2-OH dendrimer in 9.1% D_2O solution. Data shown are the addition of six 4 h accumulations during the second day of the reaction.

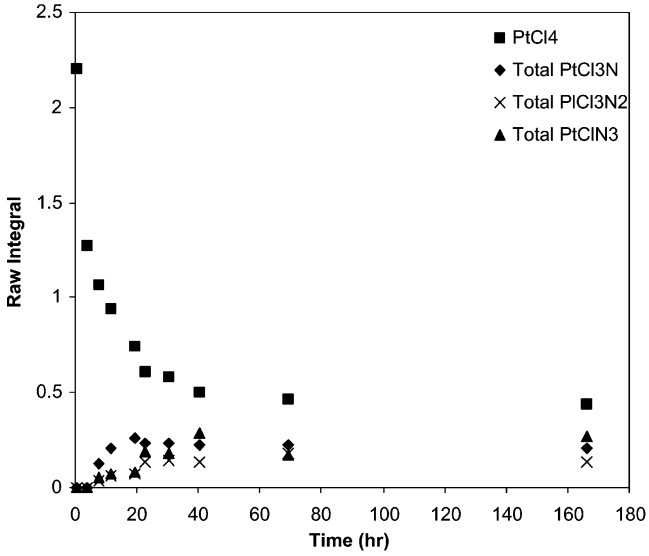

Figure 3. Peak intensities from the ^{195}Pt NMR spectra taken during the course of the reaction of 0.09 M K_2PtCl_4 and 0.009 M G2-OH dendrimer in 9.1% D_2O solution. To simplify the diagram, peak types based on the number of nitrogen atoms bound to platinum are added together.

previous assignments of the platinum anticancer drug *cis*-$Pt(NH_3)Cl_2$ bound to DNA,[20] these complex resonances are from the platinum bound to one, two, and three nitrogen atoms, respectively. Additional peaks develop over the first 24 h, and seven platinum binding environments are identified. This can be seen in the ^{195}Pt spectrum shown in Figure 2. The time dependencies of the peak intensities are summarized in Figure 3. To simplify the diagram, peak types based on the number of nitrogen atoms bound to platinum are added together. The reaction appears to reach equilibrium after 48 h.

The two resonances near −1900 ppm are attributed to Pt(II) bound to three chlorides and one nitrogen. For Pt(II), the tertiary amine nitrogen is likely the preferred binding site compared to the amide secondary nitrogen.[14,16] It has been reported that a similar dendrimer binds Cu(II) with both its amine and amide nitrogens,[21] but with a preference for the tertiary nitrogen.[22] Therefore, the more abundant resonance at −1878 ppm is assigned to platinum bound to the tertiary amine, and the smaller resonance at −1950 ppm is from platinum complexed to an amide nitrogen. All other peaks can be assigned using simple additive rules. Using the upfield shifts for the single bound platinum from the free $[PtCl_4]^{2-}$ resonance, values of −261 ppm for the amine and −333 ppm for the amide can be added in combination to predict the chemical shift.

Table 1. ^{195}Pt NMR Chemical Shift Assignments and Shift Values Calculated with the Additive Rules for the Platinum−G2-OH Dendrimer Complex[a]

	calcd shift	measd shift	diff
$[PtCl_4]^{2-}$	n.a.	−1617	n.a.
Pt(NA)	−1878	−1878	0
Pt(NH)	−1950	−1950	0
$Pt(NA)_2$	−2139	−2133	6
Pt(NA)(NH)	−2211	−2200	11
$Pt(NA)_3$	−2400	−2414	−14
$Pt(NA)_2(NH)$	−2544	−2532	12
$Pt(NH)_3$	−2616	−2625	−9

[a] Each tertiary amine (NA) causes an upfield shift of 261 ppm, and an amide (NH) causes a 333 ppm upfield shift.

Table 1 summarizes the calculated and actual peak assignments. The simple model predicts the chemical shift very well.

It is important to note that the platinum resonances bound to three dendrimer nitrogen atoms are considerably broader than the single and double bound resonances. For this arrangement to occur, it is likely based on steric grounds that nitrogen atoms from more than one "arm" of the dendrimer are involved. The motion of these platinum atoms would be much less than atoms that are attached to a single arm, which could reorient itself by either a wagging or rotating motion. For the fully encapsulated platinum atoms to reorient in solution the whole dendrimer complex must tumble. We have already shown in the case of CdS−PAMAM G4 dendrimer complexes that intradendrimer aggregation is significant.[7,11] This restricted movement combined with the large chemical shift anisotropy of platinum would cause rapid T_2 relaxation and yield broad lines.

^{1}H and ^{1}H{^{13}C} NMR Results for G2-OH. Before the platinum−dendrimer complex could be characterized by ^{1}H and indirect ^{13}C NMR, the G2-OH resonances needed to be assigned. These data are summarized in Table 2, and the following labeling system was used: Due to the repeating

$$((((HOCH_2CH_2NHCOCH_2CH_2)_2NCH_2CH_2NHCOCH_2CH_2)_2NCH_2CH_2NHCOCH_2CH_2)_2NCH_2\text{-})_2\text{-}$$

CH_2#: 1 2 3 4 5 6 7 8 9 10 11 12 13

nature of the dendrimer structure, not all of the resonances are resolved. However, the 2D NMR data show methylenes 1−8 can be uniquely assigned.

The gDQCOSY spectrum (Figure 4) shows four coupling cross-peaks between methylene pairs. The assignment starts

(20) Bancroft, D. P.; Lepre, C. A.; Lippard, S. J. *J. Am. Chem. Soc.* **1990**, *112*, 6860−6871.
(21) Ottaviani, M. F.; Bossmann, S.; Turro, N. J.; Tomalia, D. A. *J. Am. Chem. Soc.* **1994**, *116*, 661−671.
(22) Zhou, L.; Russell, D. H.; Zhao, M.; Crooks, R. M. *Macromolecules* **2001**, *34*, 3567−3573.

Table 2. ^{1}H and ^{13}C NMR Assignments of G2-OH Dendrimer and the Major Complex Structure of Complex with K_2PtCl_4[a]

	9 mM G2-OH ^{1}H δ (ppm) ^{13}C δ (ppm)	9 mM G2-OH + 90 mM K_2PtCl_4 ^{1}H δ (ppm) ^{13}C δ (ppm)	diff δ (ppm)
1	3.512 (t, J = 5.5 Hz)	3.50	−0.009
	59.9	60.2	0.3
2	3.185 (t, J = 5.5 Hz)	3.26	0.009
	41.6	41.5	−0.1
NH	−	8.06	
CO	−	−	
	175.0	171.9	−3.1
3	2.300 (t, J = 7.1 Hz)	2.76	0.46
	32.6	29.4	−3.2
4	2.687 (t, J = 7.1 Hz)	3.47	0.78
	48.9	50.4	1.5
5	2.490 (t, J = 6.8 Hz)	3.38	0.89
	51.2	52.7	1.6
6	3.163 (t, J = 6.8 Hz)	3.61	0.45
	36.8	35.0	−1.9
NH	−	8.19	
	−	−	
CO	−	−	
	174.0	173.1	−0.9
7	2.27	*b*	
	(32.6)[c]	*b*	
8	2.66	*b*	
	(48.9)[c]	*b*	
9	(2.49)[c]	*b*	
	(51.2)[c]	*b*	
10	(3.16)[c]	*b*	
	(36.8)[c]	*b*	
NH	−	−	
	−	−	
CO	−	−	
	(174.6)[c]	*b*	
11	(2.27)[c]	*b*	
	(32.6)[c]	*b*	
12	(2.66)[c]	*b*	
	(48.9)[c]	*b*	
13	*b*	*b*	
	b	*b*	

[a] Both solutions are in H_2O with 9.1% D_2O for field frequency lock. [b] Overlapped resonance unassigned. [c] Overlapped resonance assigned.

with the methylene labeled 1 (3.152 ppm) adjacent to the OH. The gDQCOSY cross-peak provides the assignment of 2 (3.185 ppm). The single bond proton−carbon correlations of the gHMQC spectrum allowed the assignment of the methylene carbon resonances. The low resolution of the gHMQC did not resolve the ^{13}C resonances of 4 from 8 and 3 from 7. However, this is not important for completing the assignments.

The methylene pairs were connected using the long-range proton−carbon correlations obtained with the gHMBC spectrum. Three bond correlations reached across the amine nitrogen to connect the methylene 4 to 5 and 8 to the overlapped resonance 9. Three bond correlations were also seen across the amide nitrogen to the carbonyl carbon from the protons of methylene 2 and 6. Two bond correlations to the carbonyl carbons with the protons of methylene 3 and 7 completed the assignment of the unique resonances. Proton and carbon resonances of 9−12 can be inferred by their similarities with those of 5−8, respectively. The assignments of 13 could not be made due to overlap and its relative low intensity. However, this assignment is not necessary for characterizing the metal−dendrimer complex.

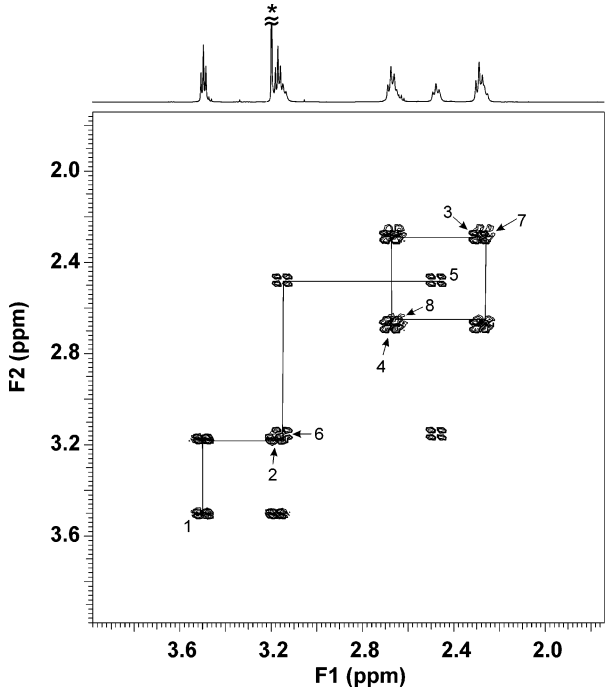

Figure 4. ^{1}H and gDQCOSY spectra of 9 mM G2-OH in 9.1% D_2O/H_2O. Peak labeled with an asterisk (*) is from methanol impurity that was carried over from the commercially delivered dendrimer.

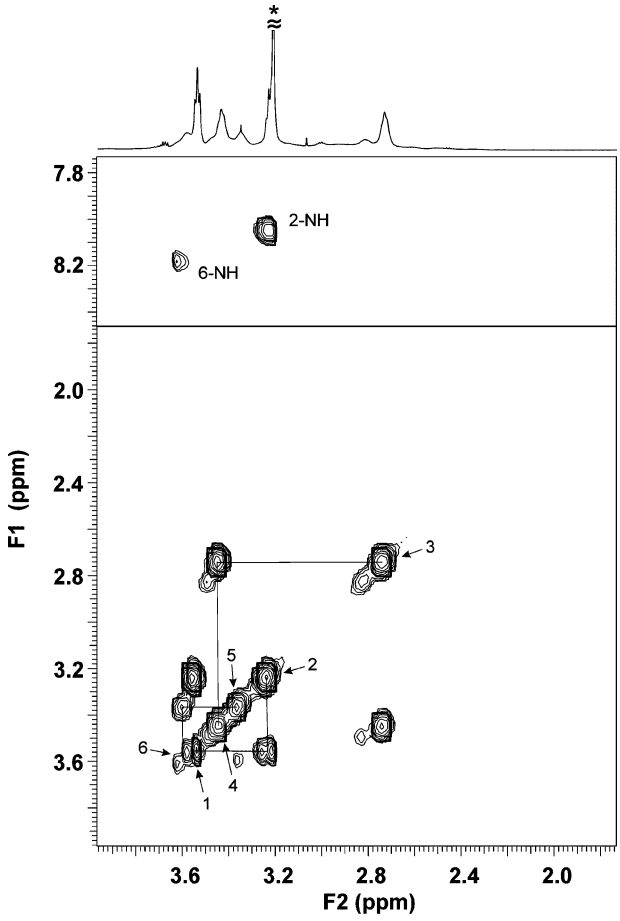

Figure 5. ^{1}H and gDQCOSY spectra of 0.09 M K_2PtCl_4 with 0.009 M G2-OH dendrimer in 9.1% D_2O solution. Peak labeled with an asterisk (*) is from methanol impurity that was carried over from the commercially delivered dendrimer.

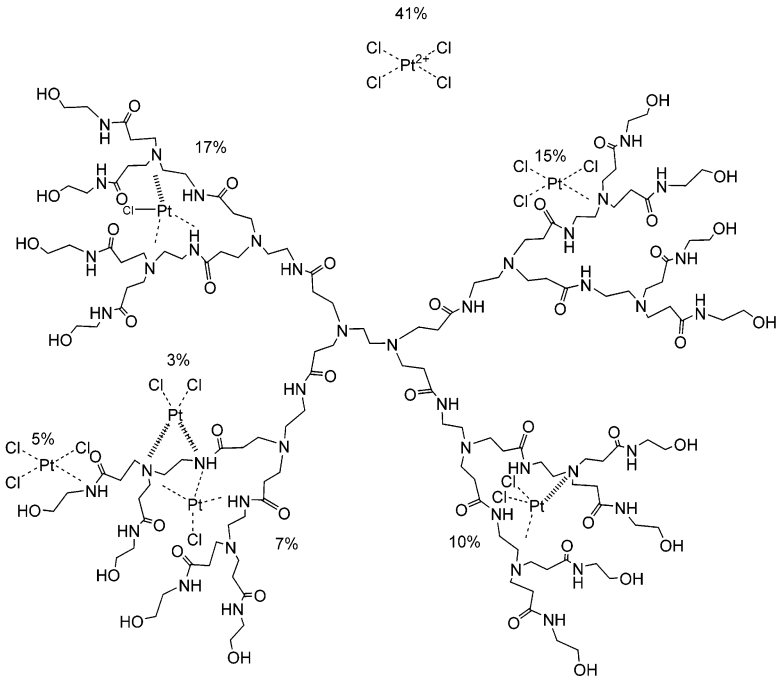

Figure 6. Summary of binding sites of Pt(II) by a G2-OH dendrimer. Percent abundance according to integration of ^{195}Pt NMR signals is indicated near each species. Tertiary amines and amide nitrogens at different branch points in the dendrimer are not distinguishable, so this picture should not be taken to mean, for example, that the innermost amide nitrogens are not coordinated to platinum ions.

The platinum−dendrimer complex structure was determined using the same methodology. Since the system is a mixture of many forms, only the major structural feature could be characterized. The gDQCOSY of the complex (Figure 5) shows cross-peaks between three methylene pairs. Additional cross-peaks between the amide protons and methylene protons 2 and 6 assist in the assignments. The correlations of the gHMQC spectrum connect the methylene protons to their carbon assignments. The same gHMBC correlations of the dendrimer (up to methylene 6) allow the connections of the three methylene pairs. Additionally, the amide proton at 8.06 ppm shows correlations to carbon 2, and carbonyl carbon at 171.9 ppm. Also, the amide proton at 8.19 ppm shows correlations to carbon 6, and carbonyl carbon at 173.1 ppm. The complete assignments are summarized in Table 2.

Inspection of both data sets in Table 2 shows that there are significant proton chemical shift differences at the methylene positions 4 and 5. This strongly supports that the tertiary amines are the predominant binding locations for platinum in the G2-OH dendrimer.

Based on the collected NMR data, we found that after 2 days of equilibration of K_2PtCl_4 with the G2-OH PAMAM dendrimer, 50% of the ^{195}Pt signal is lost, presumably as the Pt^0 precipitate. Of the remaining Pt that is still soluble, 41% remains as $[PtCl_4]^{2-}$, while 15% is bound to one tertiary nitrogen, 5% is bound to one amide nitrogen, 10% is bound to two tertiary nitrogens, 3% is bound to one tertiary and one amide nitrogen, 17% is bound to three tertiary nitrogens, 7% is bound to two tertiary nitrogens and one amide nitrogen, and 2% is bound to three amide nitrogens (Figure 6).

Binding of $[PtCl_4]^{2-}$ to G4-OH Compared to G2-OH. The complexation reaction of K_2PtCl_4 with G4-OH occurs at a slower rate than the G2-OH dendrimer, likely due to the steric crowding of the surface groups of generation 4 PAMAM dendrimers compared to the more open generation 2.[16,23] Figure 7 shows the course of this reaction followed by ^{195}Pt NMR. Only three resonances for the complexed Pt(II) are observable with chemical shifts of −1883, −2140, and −2426 ppm. These peaks are attributed to the Pt(II) bound to one, two, and three amine nitrogen atoms that are all near the surface of the dendrimers (see below).

The reaction appears to reach equilibrium after about 10 days. This observation is in accord with literature reports[1,6] as well as our own temporal measurements of Pt uptake using UV−visible spectroscopy. We also observe that the total intensity of the ^{195}Pt resonances falls during the course of the reaction to about 20% of the initial $[PtCl_4]^{2-}$ peak. However, there was no evidence of precipitation of colloidal Pt^0 during the experiment. Therefore, 80% of the Pt(II) must be sequestered deep within the G4-OH dendrimers, or the Pt(II) remains near the surface but bridges two or more dendrimers. Analogous to the G2-OH complex, the NMR signal of Pt(II) within G4-OH dendrimers will be broadened due to the T_2 relaxation caused by restriction of motion of the dendrimer as a whole. Since the G4-OH are much larger than the G2-OH dendrimers, the broadening is so severe that the peaks from the deeply bound Pt(II) are unobservable. This leads to the loss of total ^{195}Pt NMR intensity during the course of the reaction.

Of the remaining 20% of Pt(II) that provides NMR signals, 73% is still the unreacted $[PtCl_4]^{2-}$, 10% is bound to one tertiary amine, 8% is bound to three tertiary amines, 6% is bound to two tertiary amines, and 3% is bound to one water

(23) Hedden, R. C.; Bauer, B. J. *Macromolecules* **2003**, *36*, 1829−1835.

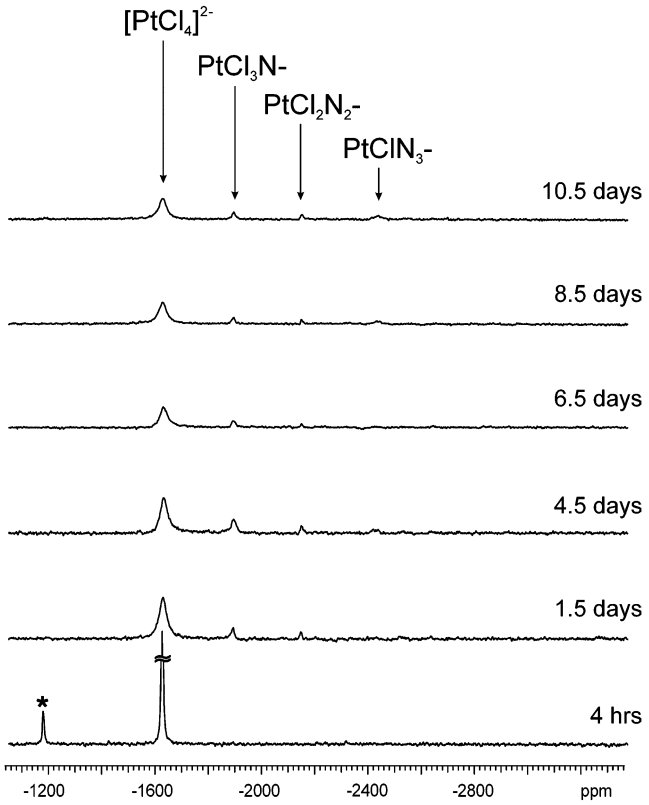

Figure 7. ^{195}Pt NMR spectra taken during the course of the reaction of 0.04 M K_2PtCl_4 added to 0.001 M G4-OH dendrimer in 9.1% D_2O solution. Peak labeled with an asterisk (*) is from $[PtCl_3OH_2]^-$, which is formed as an equilibrium product of $[PtCl_4]^{2-}$ in aqueous solution.

molecule. These assignments are based on the G2-OH results described above, with insights from ^{195}Pt NMR data taken with a platinum-containing drug and DNA.[20] The overall picture, then, is one in which a measurable fraction of the starting Pt(II) salt is unreacted, or only partially reacted, with the dendrimer. The complexation of the Pt(II) with the dendrimer not only depends on the kinetics and stability of intermediate Pt(II)−nitrogen complexes within the dendrimer, but also depends on such issues as the difficulty in putting too much charge within dendrimers and the ability of the arms of the dendrimers to coordinate to one, or more than one, Pt(II) center. In this paper, we are most interested in what environment(s) the Pt(II) is in just before it is reduced to Pt^0 to make Pt nanoparticles; clearly, the environment is complex.

AFM Measurements for G4OH−Pt_{40}. We examined the size of Pt^0 nanoparticles after reduction of G4-OH−Pt(II) complexes. Deposition of reduced, purified, diluted G4-OH−Pt_{40} solution onto cleaved mica leads to AFM topography images showing a large number of distinct features. Figure 8 shows a typical topographic image manifesting 332 distinct features. From the distribution of maximal feature heights, we obtain an average feature height of 0.98 nm. The height distribution (Figure 8) shows that the majority of the features (N = 270, 81%) have heights less than 1.2 nm. The distribution also indicates a significant number of features with heights greater than 2.0 nm (N = 9). However, the topography image does not show any evidence of fractal-like structures indicative of aggregation in solution or on the surface after deposition.

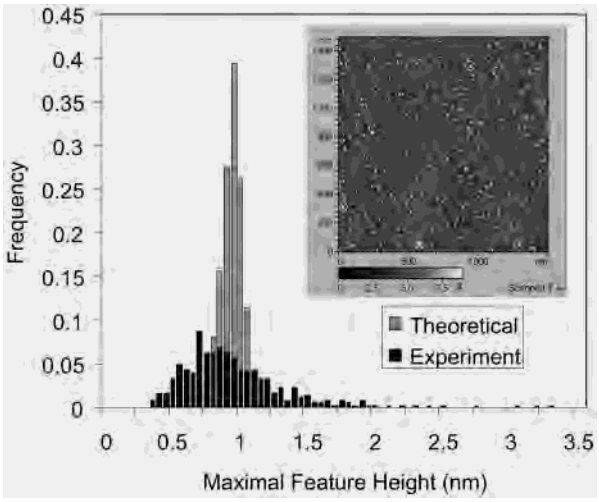

Figure 8. AFM topography image (inset) and maximal feature height distribution for G4-OH−Pt_{40} deposited onto mica. The image includes 332 distinct features with an average height of 0.98 nm. The small circles identify some of the larger features. The histogram includes the experimental distribution of feature heights (black bars) and a theoretical distribution (gray bars) described in the text.

Generating a theoretical estimate of the G4-OH−Pt_{40} feature height distribution requires several assumptions. First, we assume that the distribution of Pt(II) complexed with G4-OH (having 62 internal sites) follows a Poisson distribution with a mean of 40 Pt(II) per G4-OH. In addition, we presume a face-centered-cubic arrangement of Pt atoms in a quasi-hemispherical nanoparticle on the surface. In this scenario, the Pt nanoparticles have the theoretical distribution shown in Figure 8 with an average radius of 0.66 nm. Finally, AFM images of "empty" G4-OH on mica (not shown) suggest that the dendrimer itself adds as much as another 0.3 nm to the feature height, giving a total mean height of about 0.96 nm. Although this estimate of G4-OH−Pt_{40} feature height is close to the observed mean feature height (0.98 nm), the breadth of the measured distribution suggests other factors must play a role in determining the size of Pt nanoparticles produced by reduction of G4-OH−Pt(II) complexes and deposited on mica.

Based on the NMR data reported above, a Poisson distribution centered around 32 Pt atoms per G4-OH (80% of 40) to account for the 80% of Pt(II) that is reacted but not precipitated might be plausible. This shifts the mean of the theoretical distribution of "bare" Pt nanoparticles down to 0.61 nm, and that of G4-OH-coated nanoparticles to 0.91 nm, still in general good agreement with the AFM results (Figure 8), although the AFM data have a broader size distribution.

However, we can estimate the fraction of Pt atoms contained in features having the distribution of measured feature heights. Again, we assume quasi-hemispherical Pt nanoparticles with face-centered-cubic ordering and subtract 0.3 nm to account for the dendrimer. Under these conditions, we estimate that only 14% of the Pt atoms presumed to be in the image's features are actually in features with heights

less than 1.1 nm (the radius of a G4-OH-coated hemisphere containing 62 Pt atoms, the maximum templating capacity).

A surprising amount of Pt is captured in the relatively few, but much larger by volume, features that are larger than 1.1 nm in height. This suggests that, although much of the Pt(II) is taken up deep within or between G4-OH dendrimers, upon chemical reduction, a large proportion of the Pt(II) ends up in particles that are too large to fit inside individual dendrimers. This in turn indicates that the dendrimer may not function exactly as an "enclosed nanoreactor" that strictly templates the formation of nanoparticles within it.

Conclusion

We have followed by NMR the complexation of K_2PtCl_4 into generation 2 and generation 4 PAMAM dendrimers that bear hydroxyl groups on their surfaces. In the case of G2-OH, roughly half the Pt(II) precipitates over a 2-day period, with the remainder distributed among starting material and one, two, or three nitrogen ligands from the dendrimer. In the case of G4-OH, 80% of the Pt(II) is unobservable by NMR after 10 days, but with no precipitate; we infer that this Pt(II) is taken up deep within the dendrimer, or remains near the surface but is bridging multiple dendrimers. For G4-OH−Pt(II) complexes reduced by sodium borohydride to Pt^0 nanoparticles, 80% of the features by AFM are less than 1.1 nm in height, small enough to be within individual dendrimers. However, on an atomic basis, more Pt atoms end up in larger Pt^0 nanoparticles. Thus, the dendrimer not only acts as a template for the formation of small nanoparticles within it but also more generally acts to arrest precipitation of Pt nanoparticles that are larger than 1.1 nm.

Acknowledgment. This work was supported by the National Science Foundation NIRT Award CTS-0103135.

Supporting Information Available: gHMQC and gHMBC spectra of 9 mM G2-OH dendrimer in 9.1% D_2O/H_2O and gHMQC and gHMBC spectra of the complex formed with the addition of 0.09 M K_2PtCl_4 to 0.009 M G2-OH dendrimer in 9.1% D_2O solution. This material is available free of charge via the Internet at http://pubs.acs.org.

IC035127E